Static and Dynamic Properties of Synaptic Transmission at the Cyto-Neural Junction of Frog Labyrinth Posterior Canal

MARIA LISA ROSSI, CLAUDIO BONIFAZZI, MARTA MARTINI, and RICCARDO FESCE

From the Institute of General Physiology and the Institute of Human Physiology, University of Ferrara, 44100 Ferrara, Italy; and the Department of Pharmacology, Bruno Ceccarelli Center for the Study of Peripheral Neuropathies and Neuromuscular Diseases, University of Milano, CNR Center of Cytopharmacology, 20129 Milano, Italy

ABSTRACT The properties of synaptic transmission have been studied at the cyto-neural junction of the frog labyrinth posterior canal by examining excitatory postsynaptic potential (EPSP) activity recorded intraaxonally from the afferent nerve after abolishing spike firing by tetrodotoxin. The waveform, amplitude, and rate of occurrence of the EPSPs have been evaluated by means of a procedure of fluctuation analysis devised to continuously monitor these parameters, at rest as well as during stimulation of the semicircular canal by sinusoidal rotation at 0.1 Hz, with peak accelerations ranging from 8 to 87 deg·s^{-2}. Responses to excitatory and inhibitory accelerations were quantified in terms of maximum and minimum EPSP rates, respectively, as well as total numbers of EPSPs occurring during the excitatory and inhibitory half cycles.

Excitatory responses were systematically larger than inhibitory ones (asymmetry). Excitatory responses were linearly related either to peak acceleration or to its logarithm, and the same occurred for inhibitory responses. In all units examined, the asymmetry of the response yielded nonlinear two-sided input-output intensity functions. Silencing of EPSPs during inhibition (rectification) was never observed.

Comparison of activity during the first cycle of rotation with the average response over several cycles indicated that variable degrees of adaptation (up to 48%) characterize the excitatory response, whereas no consistent adaptation was observed in the inhibitory response.

All fibers appeared to give responses nearly in phase with angular velocity, at 0.1 Hz, although the peak rates generally anticipated by a few degrees the peak angular velocity.

From the data presented it appears that asymmetry, adaptation, and at least part of the phase lead in afferent nerve response are of presynaptic origin, whereas rectification and possible further phase lead arise at the encoder. To confirm these

Address reprint requests to Prof. M. L. Rossi, Institute of General Physiology, University of Ferrara, via Borsari 46, 44100 Ferrara, Italy.

J. GEN. PHYSIOL. © The Rockefeller University Press · 0022-1295/89/08/0303/25 $2.00
Volume 94 August 1989 303–327

conclusions a simultaneous though limited study of spike firing and EPSP activity has been attempted in a few fibers.

INTRODUCTION

The information reaching central vestibular neurons from the semicircular canal, i.e., the afferent spike-firing pattern, constitutes the result of a series of signal-processing steps. When the semicircular canal transfer function is investigated by studying afferent spike rate in response to rotation, static as well as dynamic departures are observed from the predictions of the torsion-pendulum model (Steinhausen 1931, 1933), which describes the hydrodynamic properties of the cupula-endolymph system. Static departures include asymmetry in response to excitatory and inhibitory accelerations, nonlinear intensity functions during excitation and inhibition,[1] and rectification (transient silencing of afferent discharge). Dynamic departures from the model include adaptation in response to long-lasting velocity ramps and harmonic distortions in response to sine wave stimuli (for a review, see Correia et al., 1977).

The contributions of intermediate steps occurring in the hair cell to the overall signal processing are not clear. Information is available on the mechanoelectrical transduction process: cupula displacement in the semicircular canal leads to stereocilial deflection, which in turn produces changes in hair cell membrane potential (receptor potential, Valli and Zucca, 1976). Intracellular recordings from frog canal hair cells are not available; however, data from bullfrog saccular hair cells indicate that the receptor potential is roughly linear with the extent of hair-tip displacement up to ~400 nm, and becomes asymmetrical and nonlinear for greater deflections (Hudspeth and Corey, 1977). Receptor potential presumably activates voltage- and ion-dependent basolateral conductances (Hudspeth and Lewis, 1988*a*, *b*), which ultimately result in regulation of transmitter release. However, the relation between the intensity and time course of hair cell currents and transmitter release has not been studied in detail, and little is known about the properties of synaptic transmission at the cyto-neural junction. Also unclear is the role of postsynaptic factors, such as further possible sources of membrane potential change (the activation of sodium pumping for example), which may add to the depolarization produced by the transmitter, and the properties of the encoder, which translates the resulting fluctuations in membrane potential into spike-firing rate (Fernandez and Goldberg, 1971; Precht et al., 1971; Blanks and Precht, 1976; O'Leary and Honrubia, 1976; Correia et al., 1977; Taglietti et al., 1977; Segal and Outerbridge, 1982*a*, *b*; Rossi and Martini, 1986*a*).

Crucial contribution to the understanding of vestibular function would arise from information regarding the mechanisms of transmitter release. This can be derived from the analysis of the EPSPs recorded from the afferent nerve fibers close to the synapse. The EPSPs generated at the canal cyto-neural junction are recorded together with the all or nothing action potentials. However, spike firing can be cancelled by the external application of tetrodotoxin and EPSPs can be examined in

[1] The terms excitation and inhibition as used here reflect the accepted nomenclature in vestibular literature, i.e., increase and decrease in EPSP and spike rates.

isolation (Rossi et al., 1977). By relating this approach with the traditional study of spike discharge, the characteristics of the encoder may be clarified as well. No quantitative evaluations of the EPSP parameters at rest and during rotation of the canal have been reported so far. Difficulties arise mainly from the fact that even at rest the EPSPs occur at a considerably high rate (often over 100 EPSPs$\cdot s^{-1}$) and their frequency consistently increases during the excitatory stimulation of the canal. This leads to a high degree of overlapping of the individual EPSPs, which prevents direct counting of their numbers. In this study, we decided to treat the electrical signal arising from the summation of EPSPs as "shot noise." Noise analysis was performed using a statistical procedure, based on the extension of Campbell's theorem to higher semi-invariants (Rice, 1944), which was developed to study massive neurosecretion at the frog neuromuscular junction (Segal et al., 1985), even in the presence of nonstationary rates of occurrence, nonuniform amplitudes, and nonlinear summation of the events (Fesce et al., 1986*b*). The procedure was transferred to the posterior canal cyto-neural junction with further refinements, thus yielding continuous, time-varying estimates of EPSP amplitude, h, rate of occurrence, $\langle r \rangle$, and waveform, $w(t)$. The sources of bias and error in our estimates have been considered and compensated for.

The analysis has been attempted also in a few fibers where spike firing had not been abolished, with the aim of correlating EPSP and spike behaviors.

METHODS

Electrophysiology

Experiments were performed on frogs (*Rana esculenta*, 25–30 g body weight) at room temperature (20–22°C). The posterior ampulla and its nerve were exposed in the right half of the frog head. The labyrinth, protected by its bone, was then isolated and accurately positioned at the center of a small turntable so that the posterior canal lay in the plane of rotation. The canal was stimulated by sinusoidal velocity changes at a constant frequency (0.1 Hz) with different amplitudes (20–220 deg$\cdot s^{-1}$) resulting in acceleratory peaks of increasing intensity (7.88–86.7 deg$\cdot s^{-2}$). Intracellular recordings were obtained both at rest and during rotation with glass microelectrodes filled with 3 M potassium chloride inserted into the posterior nerve within about 500 μm from the synapse. Details of the experimental and recording procedures have been extensively described in previous papers (Rossi et al., 1977, 1980; Rossi and Martini, 1986*a*, 1988). The composition of Ringer solution was (in millimolar): 117 NaCl, 2.5 KCl, 1.8 $CaCl_2$, 5 glucose, 5 Tris-HCl (pH 7.2). When the EPSPs were to be recorded in isolation 10^{-6} M tetrodotoxin (TTX, Sigma Chemical Co., St. Louis, MO) was added to the bathing medium, to prevent afferent spike activity. Data were tape recorded and then processed off-line.

All computations were performed on data recorded by a Racal 4DS tape recorder (Racal Industries Ltd, Southampton, UK), played back through a four-pole Butterworth low-pass filter (Frequency Devices, Inc., Haverill, MA) with 1.0 kHz corner frequency to avoid aliasing, and sampled at 2.0 kHz using a micro PDP-11/23 plus computer (Digital Equipment, Maynard, MA).

Fluctuation Analysis

In the presence of TTX, the electrical signal recorded intraaxonally from the ampullary nerve close to the sensory synapse is generated by the superimposition of excitatory postsynaptic

potentials (EPSPs) occurring at random. The time-varying voltage was analyzed by fluctuation analysis, using a procedure based upon Campbell's theorem and its generalization by Rice (1944) to higher semi-invariants. The generalized theorem states that, if a fluctuating potential is generated by summation of randomly occurring elementary events described by the product $h \cdot w(t)$, where t is time, h is the amplitude parameter, and $w(t)$ is a dimensionless function of time which describes the waveform of the event, then we have:

$$\text{Mean} = \langle r \rangle \cdot h \cdot \int w(t)\, dt \tag{1}$$

$$\text{Var} = \langle r \rangle \cdot h^2 \cdot \int w^2(t)\, dt \tag{2}$$

$$\text{Skew} = \langle r \rangle \cdot h^3 \cdot \int w^3(t)\, dt \tag{3}$$

where $\langle r \rangle$ is the mean rate of occurrence and Mean, Var, and Skew are the first three semi-invariants of the distribution of the values of the time-varying potential.

Eq. 1 cannot be used in our experiments because during prolonged recordings the mean value (membrane potential) may be affected by factors other than EPSP summation, and in our recordings DC components may be masked by capacitive coupling. Still, Eqs. 2 and 3 hold. Thus $\langle r \rangle$ and h can be easily computed, once the waveform $w(t)$ of the EPSP is known. The waveform is deduced by fitting the power spectrum of the fluctuating potential, based on the equation:

$$G(f) = 2\langle r \rangle \cdot h^2 \cdot |W(f)|^2 \tag{4}$$

where $G(f)$ is the power density of the recorded signal and $W(f)$ is the Fourier transform of $w(t)$. EPSP amplitude and rate are then deduced from the following relations:

$$h = (\text{Skew}/\text{Var}) \cdot (I_2/I_3) \tag{5}$$

$$\langle r \rangle = (\text{Var}^3/\text{Skew}^2) \cdot (I_3)^2/(I_2)^3 \tag{6}$$

where I_2 and I_3 represent the integrals of the square and the cube of $w(t)$, respectively (Segal et al., 1985).

Eqs. 1–6 were originally derived based on the assumptions of a point, stationary, and uniform Poisson process, generated by uniform and uncorrelated events, occurring at random, at a stationary mean rate, and summing up linearly. These constraints are violated by the biological process under study.

Nonstationarity and correlations among the events contribute to the variance, the skew, and the power spectrum. Rigorous analyses of the power spectrum of processes that are not ergodic (Schick, 1974) or where the parameters of the events are correlated (Heiden, 1969) indicate that the spectrum is always given by one factor with the same frequency composition as the single event (i.e., $G(f)$ in Eq. 4) and an "interference" factor contributed by nonstationarity and/or correlation. The spectrum has the expected shape (as described by Eq. 4) over a defined region (say, between f_1 and f_2), only when the interference factor is negligible within this region. Under these conditions, the elimination of frequency components outside the region $f_1 < f < f_2$ effectively removes the contributions of nonstationarity and correlations to the power spectrum, variance and skew of the noise (Fesce et al., 1986*b*). Therefore, Eqs. 1–6 hold after appropriate filtering of the signal (a 1-ms RC highpass filter was used here).

Nonuniform amplitudes of the EPSPs cause an overestimate of h as obtained from Eq. 5, because $\langle h^3 \rangle / \langle h^2 \rangle$ is greater than $\langle h \rangle$, and an underestimate of $\langle r \rangle$ from Eq. 6. These biases can be easily corrected for if the shape of the distribution of EPSP amplitudes is known. To this purpose, histograms of the distribution of EPSP peak amplitudes were obtained from a few units. Portions of the experiments where EPSP rate was low enough to resolve individual events were analyzed. Digitized records of membrane potential at rest as well as during stimulations of various amplitudes were displayed, and the peak amplitudes of ~300 EPSPs were

measured for each histogram. The baseline for an individual EPSP was determined either by linearly extrapolating the values that prevailed just before it occurred or by joining the values before and after it. Events with notches and inflections on their rising phases were counted as multiple events. Amplitudes could not be measured reliably on single events when EPSP rate exceeded 100 s^{-1}. If the waveforms of the events are not correlated with their amplitudes, within the same unit, then the peak amplitude is proportional to h and the two parameters have the same distribution.

Nonlinear summation of the EPSPs, due to the nonlinear conductance-voltage relation of the membrane, introduces bias in our estimates, although they are based on the fluctuations of the membrane potential about its mean value (a few millivolts), disregarding the much larger changes in mean membrane potential. The main effect of nonlinear summation is to reduce the skewness of the signal (Fesce et al., 1986*b*), yielding underestimated h and overestimated $\langle r \rangle$. At the endplate, these errors were significant for miniature endplate potential rates >500 s^{-1} (Fesce et al., 1986*a*); however, it was shown that Martin's correction factor (Martin, 1955) was adequate to recover corrected values for the semi-invariants, yielding valid estimates of $\langle r \rangle$ and h (Fesce et al., 1986 *a*, *b*). In particular, the relation, $v_l = v/(1 - v/V_d)$ (Martin, 1955), is used, where v is the displacement of membrane potential from its mean value, v_l is the linearized displacement, that would occur if the voltage/conductance relation were linear, and V_d is the driving potential across the EPSP channel. Variance and skew can be "linearized" according to the following equations (Fesce et al., 1986*a*):

$$\mathrm{Var}(l) = \mathrm{Var}(m) + 2 \cdot \mathrm{Skew}(m)/V_d$$

$$\mathrm{Skew}(l) = \mathrm{Skew}(m) + 6 \cdot [\mathrm{Var}(m)]^2/V_d + 3 \cdot \lambda_4/V_d$$

where Var(l) and Skew(l) are the values of variance and skew that one would measure in a linear system, Var(m) and Skew(m) are the measured values, and λ_4 is the fourth semiinvariant of the fluctuations. According to Eqs. 2 and 3, Skew = $\langle r \rangle h^3 I_3$ = Var·h·I_3/I_2, and Var^2 = $\langle r \rangle^2 h^4 I_2^2$ = Skew·$\langle r \rangle h(I_2^2/I_3)$; similarly, $\lambda_4 = \langle r \rangle h^4 I_4$ = Skew·hI_4/I_3, where I_4 is defined as I_2 and I_3 (Rice, 1944). Therefore we have, to a first approximation:

$$\mathrm{Var}(l) = \mathrm{Var}(m)[1 + 2 \cdot (h/V_d) \cdot (I_3/I_2)]. \tag{7}$$

$$\mathrm{Skew}(l) = \mathrm{Skew}(m)[1 + 6\langle r \rangle \cdot (h/V_d) \cdot I_2^2/I_3 + 3 \cdot (h/V_d) \cdot I_4/I_3]. \tag{8}$$

EPSP Waveform

The waveform of the EPSPs was analyzed by two different approaches: (*a*) by digitally averaging 20–30 EPSPs and fitting an analytical function to the average waveform, when EPSP rate was so low that isolated events could be found, or (*b*) by fitting the power spectrum of the voltage noise generated by the superimposition of EPSPs occurring at relatively high rates. Single events were acquired by the computer through a recursive trigger routine,[2] and examined individually before averaging. Only events resolved over their whole timecourse without overlap with other events were considered.

The waveforms of the EPSPs recorded intraaxonally varied noticeably among different experiments. However, in all cases both the averaged waveform and the power spectrum were well fit by a gamma distribution function, i.e., by the waveform:

$$w(t) = (t/\tau)^\gamma e^{-t/\tau}/\Gamma(\gamma + 1) \tag{9}$$

[2] The computer detected an event when the AC-coupled signal (time constant ~0.2 s) crossed the chosen threshold (usually ~0.2 mV above the mean baseline value) with a positive derivative greater than a fixed value (usually 0.5 V/s). The events were synchronized for averaging on the point of maximum derivative.

where τ is a time constant, γ is a shape factor, and Γ is Euler's gamma function, introduced as a normalization factor. This kind of equation, with integer values only for γ, was used to fit the waveform of depolarizing bumps in photoreceptors of *Limulus* (Fuortes and Hodgkin, 1964; Wong and Knight, 1980). The waveform shifts from a single exponential ($\gamma = 0$) to a Gaussian curve ($\gamma \to \infty$), reproducing rather closely the various degrees of cable deformation of a presumably exponential EPS current. The values of γ and τ were obtained from the time to the peak and the integrals of the averaged EPSPs based on the following equations:

$$d/dt\ w(t) = 0 \text{ for } t = \gamma\tau \text{ (time to the peak)}$$

$$\int h \cdot w(t) t^n\, dt = h\tau^{(n+1)} \cdot \Gamma(\gamma + n + 1)/\Gamma(\gamma + 1).$$

Alternatively, the same parameters were obtained from the power spectrum of the membrane voltage recording, given by Eq. 4:

$$G(f) = 2\langle r \rangle \cdot h^2 \cdot |W(f)|^2 = 2\langle r \rangle (h\tau)^2 \cdot [1 + (2\pi f\tau)^2]^{-(\gamma+1)} \quad (10)$$

On log-log plots, this spectrum has one horizontal asymptote at the low frequencies and a second asymptote at the high frequencies, which has a slope of $-2(\gamma + 1)$ and crosses the horizontal asymptote at the "corner" frequency $f_c = 1/(2\pi\tau)$. The two asymptotes were fit by shifting them and changing the slope of the high frequency one, while the computer displayed (*a*) the resulting curve, superimposed on an oscilloscope screen with the data spectrum and (*b*) the error between fit and experimental points. When the best fit was obtained, as judged by eye, the value of γ was derived from the slope of the high frequency asymptote and the value of τ was derived from the crossing frequency. Power spectra were computed from eight contiguous records, each record containing 2,048 12-bit data points collected at 2.0 kHz. The ends of each digital record were cosine tapered to reduce leakage of spectral components due to windowing (Bendat and Piersol, 1971), and a fast Fourier transform was performed. The eight resultant spectra were averaged, the average was fit as described, and final plots were obtained after further smoothing over frequency (Segal et al., 1985).

An EPSP with the fit waveform was simulated by the computer and output as an analog signal, passed through the same filters used for data acquisition (i.e., the antialiasing low-pass filter and a 1-ms RC highpass filter, see above), and sampled and converted back to digital form. The computer then evaluated the integrals of the square and cube of $w(t)$, as modified by the filters, to be introduced in Eqs. 5 and 6 for the computation of EPSP rate and amplitude. EPSP waveform was fit and values for I_2 and I_3 were computed for each unit at rest and at least once during each rotation.

Computation of EPSP Rate and Amplitude

In previous applications of the procedure of fluctuation analysis values for the rate and the amplitude of the elementary events were computed from Eqs. 5 and 6 using the variance and the skew measured on successive records of either 10 s (Segal et al., 1985; Haimann et al., 1985; Fesce et al., 1985*a*) or 5 s duration (Ceccarelli et al., 1988). We were interested in a much faster resolution of changes in EPSP rate and amplitude, so we decided to use a moving average procedure to compute the variance and skew of the fluctuating potential as continuous functions of time. After fixing the mean value to zero by high-pass filtering the signal through a 1-ms RC, a square window was used to obtain a moving average of the squared and cubed signal. This was performed by the computer during data acquisition from the tape recorder. The measured changes in EPSP rate from its resting value were directly compensated for the phase shift (half the window duration) and the attenuation of periodic changes due to a window duration of half a period (attenuation = $2/\pi$) or one-fourth of a period ($2 \cdot \sqrt{2}/\pi$).

The resulting "instantaneous" values of Var and Skew were used in Eqs. 5 and 6, together with appropriate values for I_2 and I_3, computed by linear interpolation between the values measured at different times. Continuously varying estimates of EPSP rate and amplitude were thus obtained. The computer output such estimates as an analog signal, which was displayed and saved by means of a chart recorder (model 28000; Bryans Southern Instruments Ltd., Mitcham, UK) together with the simultaneous recording of the stimulus, i.e., the turntable angular velocity.

The relative constancy of the estimated values of EPSP amplitude within a single recording was considered as an indicator of the consistency of the analysis procedure and adequacy of sample size (i.e., averaging period) in the measurement of the time varying variance and skew. However, random errors of the estimates are of little concern here, because they simply give some excess oscillations in the continuous estimates of EPSP rate and amplitude.

The results were compared with direct EPSP counts and amplitude measurements when the rate was low enough to resolve individual events, and the adequacy of the running averaging procedure was tested on simulated data (see Appendix).

RESULTS

The EPSP activity recorded in the presence of TTX at rest and during sinusoidal canal rotation from a unit of the posterior nerve is illustrated in Fig. 1. In the figure

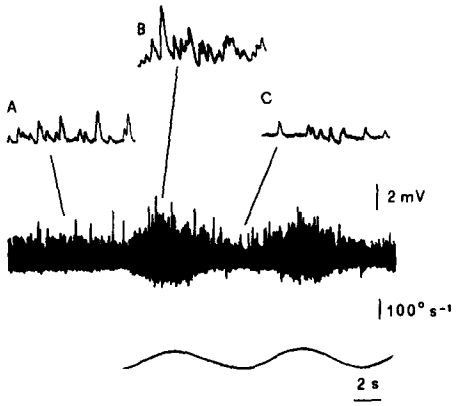

FIGURE 1. Oscilloscope tracings of the fluctuations in membrane potential recorded from a posterior canal afferent axon at rest and during sinusoidal rotation at 0.1 Hz (40 deg·s^{-2} peak acceleration) in the presence of TTX. The angular velocity of the turntable is displayed below to mark the period of stimulation. Portions of the recording (100 ms duration) are shown with an enlarged time scale in the insets: (*A*) spontaneous activity, (*B*) excitatory acceleration, (*C*) inhibitory acceleration. Vertical bar = 2 mV (all records).

insets, enlarged tracings from the same unit show EPSPs at rest (*A*) and at the maximum excitatory and inhibitory responses (*B* and *C*, respectively). Overlapping of EPSPs is evident both at rest and during rotation.

The Waveform of the EPSPs

Examples of power spectra obtained from similar recordings, at rest and during stimulation, are shown in Fig. 2. The spectra consistently demonstrated a horizontal asymptote at the low frequencies, a single corner, and an asymptote at the high frequencies with variable slope, as predicted by Eq. 10, which always gave a good fit to the spectra. This suggests that gamma distribution functions accurately describe the waveforms of the individual events that generate the electrical noise recorded in our experiments. The values of τ computed from the power spectra in all the units

studied (8) ranged between 0.55 and 1.25 ms, and the values of γ ranged between 0.8 and 1.8. The values computed in the same unit at rest and during sinusoidal stimulation were consistent and never showed variations >20%. Often the spectra showed a slight downward displacement of the first few points, at the low frequency end. This could be due either to capacitive coupling during recording or to correlation among the events (Wong and Knight, 1980), but this did not interfere with the results of our further analysis (Fesce et al., 1986*b*), which was performed on recordings high-pass filtered through a 1-ms RC filter (~160 Hz corner frequency).

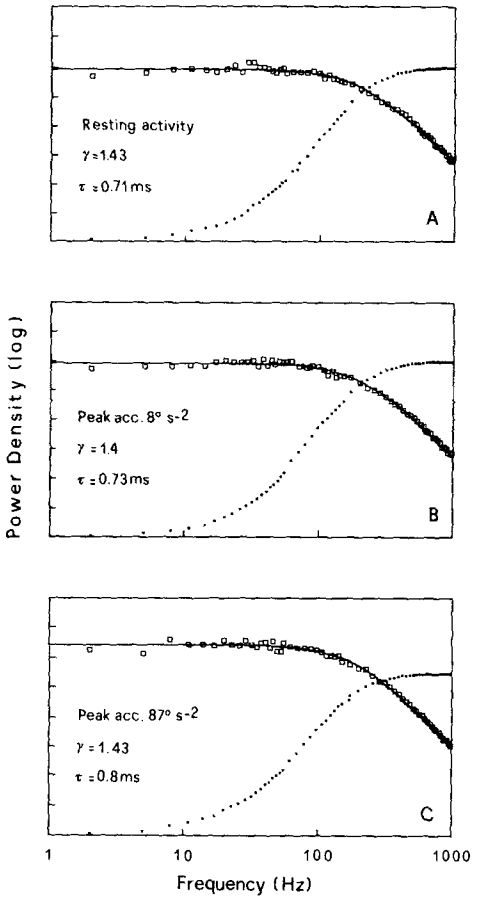

FIGURE 2. Power spectra of the fluctuating membrane potential computed from a single unit at rest (*A*) and during sinusoidal rotation at 0.1 Hz, with peak accelerations of 8 (*B*) and 87 deg·s^{-2} (*C*). *Squares*, experimental data points (frequency smoothed averages of eight spectra from 2,048 points each) on free logarithmic scale. Continuous lines, spectra of the gamma distribution functions best fitting the data (values of the parameters γ and τ of the fits are indicated on each panel). *Dots*, integrals of the power spectra (free linear scale) illustrating the relative contributions of the various ranges of frequency components to the total power (variance).

In all cases where EPSP rate was low enough to resolve individual events, EPSP waveform was studied from averaged events (10–50) as well, and estimates were obtained for the amplitude parameter h, the duration parameter τ and the shape parameter γ.

The adequacy of the chosen analytical function in describing the time course of the single event was further examined by means of a test of causality known as "minimum-phase" property (Papoulis, 1962; Wong and Knight, 1980). A waveform is minimum phase if its Fourier transform is the exponential of a causal transfer func-

tion. Because the imaginary part of a causal transfer function can be deduced from its real part (see Papoulis, 1962; Peterson and Knight, 1973), for a minimum-phase waveform the knowledge of the amplitude of the Fourier transform yields its phase. An efficient algorithm was developed by Peterson and Knight (1973) to reconstitute the waveform from the amplitude information alone, and therefore also from the power spectrum of the noise (Wong and Knight, 1980).

The average of 27 EPSPs is shown in Fig. 3 *A*. The Fourier transform of this record was computed, the phase information was discarded and the waveform was

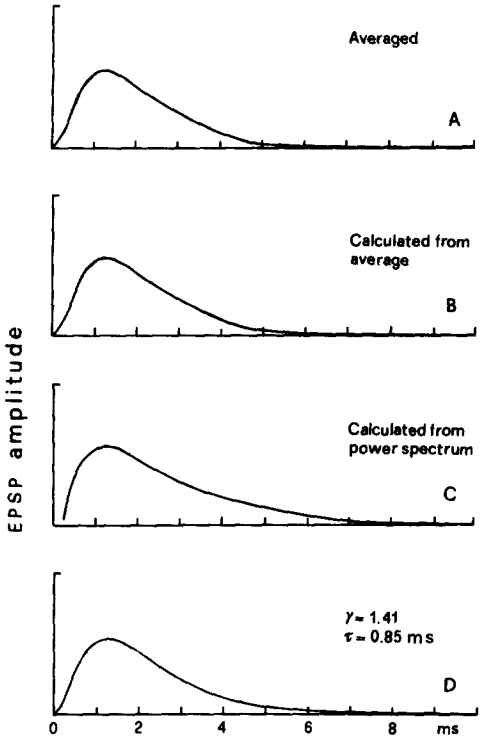

FIGURE 3. Analytical reconstruction of EPSP waveform. (*A*) average of 27 EPSPs recorded from the same unit at rest and during inhibition. (*B*) waveform reconstituted from the amplitude of the Fourier transform of the record in *A* (i.e., neglecting phase information) using an algorithm based on the assumption of a "minimum phase" waveform; the excellent reproduction of the record in *A* validates the assumption. (*C*) waveform obtained by the same algorithm as in *B*, using the power spectrum of the fluctuations in membrane potential computed from the same recording from which the EPSPs averaged in *A* were extracted. The reasonably good reconstruction of EPSP waveform indicates that the noise is constituted by shots occurring at random and with the same waveform as the isolated EPSPs, and that possible correlations, nonstationarity and nonuniformity of the events are not prominent. (*D*) Analytical waveform of the EPSP (gamma distribution function) obtained using the values of the parameters γ and τ giving best fits to the averaged EPSP and the power spectrum.

reconstructed by means of the cited algorithm, assuming the minimum-phase property. The reconstituted waveform (Fig. 3 *B*) is in close agreement with the experimental waveform, which validates the minimum-phase postulate for EPSP waveform. Alternatively, the same algorithm was applied to the power spectrum of noise recorded at the same unit, neglecting the information acquired from single events: the waveform in Fig. 3 *C* was obtained, which also agrees rather well with *A*. The main departures of the reconstructed waveform from the single event shape regard the initial foot and the tail, i.e., are confined to low frequency components. This is

in accord with the observed departures of experimental spectra from Eq. 10, always limited to the low frequency region. Therefore, high-pass filtering will eliminate deviations (presumably due to nonstationarity and/or correlations) yielding a signal that behaves like shot noise produced by the summation of uncorrelated single events, with the same waveform as the isolated EPSP, occurring at random and at a stationary mean rate. Furthermore, a good fit is obtained both to the averaged EPSP and to the power spectrum (not shown) using the gamma distribution function with $\tau = 0.85$ ms and $\gamma = 1.41$ to describe the EPSP waveform (Fig. 3 *D*). The agreement of minimum-phase algorithm and direct fitting with each other justifies the use of the simpler method of fitting gamma distribution functions (Eqs. 7 and 10) to averaged EPSPs and spectra. Notice that gamma distribution functions possess the minimum phase property.

To evaluate the variations in the waveforms of different events within the same unit, in a few experiments we fit gamma distribution functions to single events as well. The coefficients of variation (cv^2 = var/mean^2) observed for the parameters of EPSP waveform within single units were 0.04–0.3 for γ, 0.012–0.17 for τ, 0.13–0.15 for h; similar variations were observed in the integrals of the square and cube of EPSP waveform (I_2 and I_3, used for the computation of EPSP rate and amplitude, see Methods). No statistically significant correlation was found between the amplitude parameter h and either τ ($r = -0.48$ to -0.69) or γ ($r = 0.53$–0.78), although the values of the correlation coefficients and visual inspection of the data suggested that there might be a tendency to observe shorter apparent durations and less sharply peaked shapes for the higher events. Such lack of statistically significant correlations implies that no significant contributions to the variance, skew and power spectrum are generated by correlation, which is in accord with the good agreement of experimental power spectra with the analytical predictions (see above).

The Amplitude Distribution of the EPSPs

Histograms of the distribution of the peak amplitudes of EPSPs were computed from four units during spontaneous activity as well as during sinusoidal rotations of different amplitudes. Each histogram was constructed from 240–380 events; a total of 3,500 EPSPs were analyzed. The mean peak amplitude of EPSPs ranged in the various units between 0.8 and 1.3 mV. A representative sample of histograms computed from a single unit is illustrated in Fig. 4. Coefficients of variation of 0.19–0.23 were computed for this unit, and in general values from 0.12 to 0.29 were observed in all units. The distribution is clearly skewed toward the higher values because of the presence of "giant" events, whose occurrence can often be recognized by visual inspection of the recording. The distribution of EPSP amplitudes in this unit would yield ratios $\langle h^3\rangle/\langle h^2\rangle = 1.46$ and $\langle h^2\rangle^3/\langle h^3\rangle^2 = 0.59$, thus leading to overestimating the h parameter by 30% and underestimating $\langle r\rangle$ by 40%. The bias so evaluated varied <5% among the various histograms computed from the same unit. Taking together the data from the four units analyzed, values of h turn out to be biased by $+0.40 \pm 0.08$ and values for $\langle r\rangle$ by -0.40 ± 0.08 because of nonuniform amplitude of the EPSPs. Because the resulting correction factors were virtually constant for single units under various conditions of stimulation, and they did not vary much (<10%) among the different units, we decided to apply a uniform correc-

tion (0.7 for h and 1.64 for $\langle r \rangle$) to the results from all units. As it will be discussed below, this bias is partly compensated by bias in the opposite direction introduced by the nonlinear summation of the events.

Estimates of Resting Potential and Nonlinearity

Recordings were obtained in 18 units before applying TTX, so that action potentials could be studied together with EPSPs. The amplitude of the spikes ranged in the various units between 30 and 60 mV. Assuming a resting potential (V_m) in the order of −80 mV, the real amplitude of the spikes should be 90–100 mV, suggesting that an attenuation factor close to 2 affected our recordings. The mean peak amplitude of isolated EPSPs ranged between 0.9 and 2.3 mV and in each unit it was well correlated with the amplitude of the spike (slope = 0.038, intercept = 0.11 mV, and r =

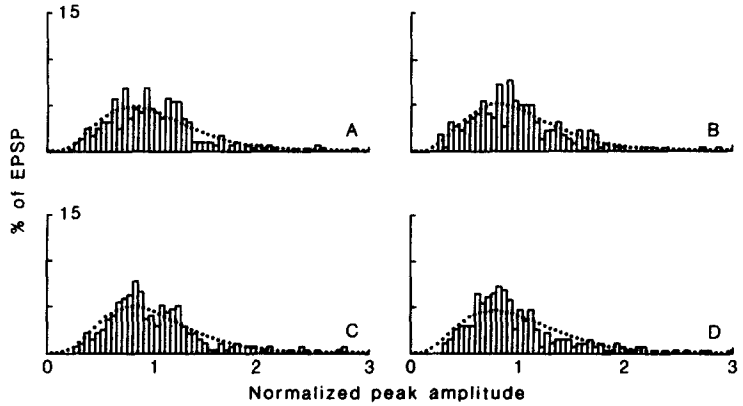

FIGURE 4. Distribution histograms of the peak amplitude of single events measured on portions of the recordings from a single unit. (*A*) Spontaneous activity. (*B*, *C*, and *D*) Sinusoidal rotations of 0.1 Hz, with peak accelerations of 16, 40, and 87 deg·s^{-2}, respectively. The amplitudes were normalized in all histograms, since the correction factors derived from these histograms are independent of the mean values (see text). Mean values were 1.11, 1.22, 1.10, and 1.07 mV in the four conditions presented. The dotted lines are gamma distribution functions computed from the coefficient of variation of each histogram; they fit well the observed distributions, which can therefore be considered unimodal and continuous.

0.95 by linear regression). Since it is unlikely that the EPS current and spike sodium current have the same reversal potential, the intercept close to 0 mV suggests that differences in EPSP peak amplitude among the various units are not due to differences in V_m, but rather to the differences in recording conditions (input impedance and location of the recording electrode, capacitive coupling) that affect spike amplitude as well. The slope of the mentioned linear regression indicates a real EPSP amplitude of 4–5% of the resting potential in all units, i.e. 3.5–4 mV.

If the reversal potential for the channels whose openings produce an EPSP is close to zero, then the driving potential across the channels (V_d) can be tentatively set close to V_m (80 mV). The range of values obtained for EPSP waveform parameter γ in our experiments implies that the amplitude parameter h is close to three

times the EPSP peak amplitude. The amplitude parameter h would therefore be about 14% of the driving potential, and the ratio h/V_d would be 0.14. Since in our experiments I_3/I_2, I_2^2/I_3, and I_4/I_3, took values ~0.25, 0.7 ms, and 0.25, respectively, Eqs. 7 and 8 indicate that the variance was underestimated by ~7%, and the skew by a factor of $\sim 1 - 1/(1.1 + \langle r \rangle/1{,}700)$ because of nonlinear summation.

Estimates of h must therefore be corrected by a factor of $(1.03 + \langle r \rangle/1{,}800)$, and estimates of $\langle r \rangle$ by $(1.05 + \langle r \rangle/1{,}800)^{-2}$, where $\langle r \rangle$ is the corrected value. At the maximum rates here observed (~1,000 s^{-1} uncorrected rate), the correction factors for nonlinear summation reached values of 1.33 for h and 0.55 for $\langle r \rangle$. Data reported in the following sections have been corrected both for nonlinear summation and for the distribution of amplitudes. The two corrections tended to cancel each other, being of similar magnitude, in opposite directions (see also Fesce et al., 1986*a*). This can be appreciated by inspection of the two scales, uncorrected vs. corrected rate, in Fig. 5.

Measurements of EPSP Amplitude at Rest and during Rotation

Among the data obtained from 18 units, 8 units were selected for further analysis, from which a continuous recording free of artifacts and variations in apparent resting potential had been obtained during 2–3 min of resting activity and at least four successive cycles of sinusoidal rotation at 0.1 Hz with four different amplitudes.

The amplitude parameters (h) measured by fluctuation analysis in these units ranged between 2.5 and 4.5 mV, which corresponds to mean peak amplitudes of the events of 0.74 to 1.38 mV (as computed from h and the value of γ). These figures agree well with the range of mean peak amplitudes directly measured on histograms of single events (0.8 to 1.3 mV, see above), so validating the statistical procedure used. Within single units, the time varying estimates of h remained fairly constant during the periods of stimulation. Jumps and rapid fluctuations in time were sometimes produced in the continuous tracings of h by the occurrence of giant events, particularly during strong accelerations. Apart from these brief artifacts, the fluctuations in the recordings of h, which yield an indirect estimate of random errors affecting our measurements, remained rather small (<10%). Examples of continuous measurements are shown in Fig. 5 (upper traces in *A–D*).

Measurements of EPSP Rate during Excitatory Rotation

The resting EPSP frequency in the units under study ranged between 50 and 280 s^{-1}. No consistent relation was found between resting rates and magnitude of the response. In units with resting rates up to 100 s^{-1}, the ratio of EPSP rates as measured by fluctuation analysis to the numbers of directly counted EPSPs per second was 1.00 ± 0.18 (SD; sixteen 3–7-s intervals from four units).

Six of the eight units were subjected to rotatory accelerations of 8 deg·s^{-2}. In four of these units, the change in EPSP frequency approximately followed the shape of the sinusoidal stimulus applied to the receptors, whereas in the others no periodic response was detected.

On increasing the sinusoidal stimulus intensity, the response became definitely sinusoidal in all the units examined, more or less symmetrical about the resting level,

the excitatory response being roughly as conspicuous as its inhibitory counterpart, for accelerations not higher than 30 deg·s^{-2}.

On further increasing acceleration up to 87 deg·s^{-2} a marked asymmetry of the response became evident, excitation being systematically more conspicuous than inhibition. Fig. 5 shows the results of noise analysis in a typical unit. This unit started

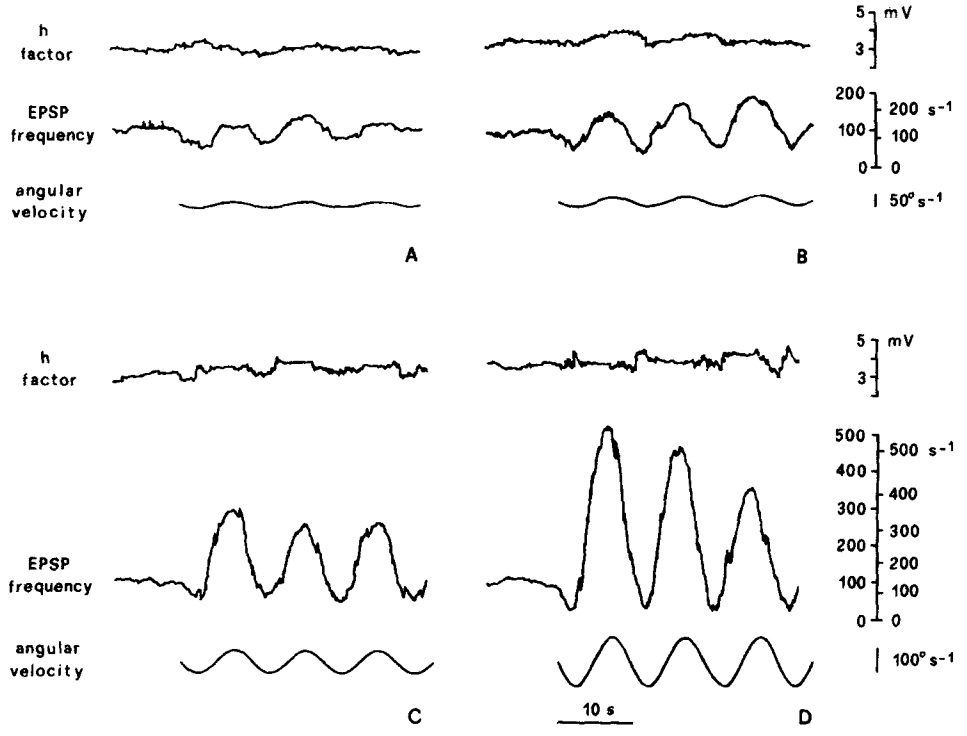

FIGURE 5. Measurements of EPSP amplitude parameter h (*upper traces*) and rate of occurrence $\langle r \rangle$ (*middle traces*) from a single unit at rest and during sinusoidal rotation at 0.1 Hz with peak accelerations of 8 (*A*), 16 (*B*), 40 (*C*), and 87 deg·s^{-2} (*D*). Bottom traces illustrate the turntable angular velocity to mark the period of stimulation. Values of h should be corrected, due to distributed EPSP amplitudes and nonlinear summation, by a factor ranging from 0.7 for $\langle r \rangle \rightarrow 0$ to 0.9 for the maximum observed $\langle r \rangle$ (500 s^{-1}). Left and right scales for $\langle r \rangle$ refer to uncorrected and corrected values, respectively; notice that the corrections for amplitude distribution and nonlinearity roughly compensate each other. Notice the wide range of modulation of EPSP rate. Notice also the marked asymmetry, and the adaptation already present in the response to the second cycle, for peak accelerations of 40 deg·s^{-2} or larger. The response parameters of this unit, which are all linear with respect to peak acceleration, are illustrated in Fig. 7 *A*.

from a resting EPSP rate close to 100 s^{-1} and could be induced to secrete up to 500 EPSPs·s^{-1} during excitatory stimulation at 87 deg·s^{-2}, slowing down to 10 s^{-1} during inhibition.

A further aspect of the pattern of EPSP response becomes evident on examining prolonged rotations: variations in EPSP rate undergo a progressive decrease. We

decided to name such rundown of the response "adaptation," as this term has been used to describe the rundown of both receptor potential response (Eatock et al., 1987) and spike response (Precht et al., 1971; Rossi and Martini, 1986*a*). Adaptation began to appear for accelerations of 40 deg·s^{-2}, and increased on increasing the stimulus intensity up to 87 deg·s^{-2}. In the illustrated unit the excitatory peak response progressively declined from its higher initial value (Fig. 5, *C* and *D*), and this was commonly observed in all units examined. As regards inhibition, on the contrary, no consistent adaptation of the decrease in EPSP rate was observed.

With increasing accelerations, the responses became larger and in the most sensitive units up to 8 s of the 10-s sinusoidal cycle appeared to be spent at EPSP rates higher than the resting level, resulting in an apparent 8-s excitatory /2-s inhibitory cycle, with a general time course of the response described by a symmetrical sinusoid centered on a mean rate higher than the resting level. One would instead expect a 5-s excitatory /5-s inhibitory response, described by an asymmetrical sinusoid with a positive lobe larger than the negative one. Actually, the observed behavior might be artifactual: the analysis of simulated data (see Appendix) indicates that smoothing an asymmetrical sinusoid over a half cycle yields a shifted symmetrical sinusoid, with the same maxima, minima, and positive and negative areas with respect to the resting level, thus spending more time at positive than at negative values. Simulation also indicates that a shorter window duration (2.5 s = one-fourth of a period) yields a more accurate description of an asymmetrical response, although the resulting continuous estimates of EPSP rate are affected by much more prominent fluctuations. When data obtained with strong accelerations were reanalyzed using a 2.5-s window, it clearly appeared that the time occupied by the excitatory and inhibitory responses were indeed roughly equal (a 6-s apparent excitatory duration was obtained in the most extreme case). Thus the actual EPSP response is described by an asymmetrical sinusoid, with a positive lobe larger than the negative one. In the three units analyzed with both window durations (2.5 and 5 s), the estimated parameters of EPSP activity (see below) did not vary in any consistent fashion, indicating that smoothing by a 5-s window did not introduce biases in the parameters under study. The variations observed between the estimates (±5–20%) are presumably due to the larger random errors introduced by the shorter averaging period, as suggested from the wider fluctuations seen in h as well. An example of the results obtained with this shorter averaging time is shown in Fig. 6.

The response in EPSP rate was described by evaluating the following parameters, normalized to the resting activity levels: (*a*) the excitatory and inhibitory peaks during sinusoidal rotation (i.e., maximum and minimum EPSP rates); (*b*) the total number of EPSPs occurring during the excitatory and inhibitory periods of the sinusoidal cycle. Because the cupula-endolymph system essentially behaves as a lowpass R.C. filter with a 1.7-s time constant (Bernard, 1982; Rossi and Martini, 1986*b*), the first 5 s of stimulation were neglected, to allow for equilibration of the system. Rotation was always started with zero angular velocity and inhibitory acceleration, so that the 5-s transient occurred during inhibition and the first excitatory peak was little affected.

Linear relations were observed in four units between excitatory stimulus and response. In these linear units, the gain of the response was computed by correlat-

ing either the peak rates or the total numbers of EPSPs during the excitatory phase of the sinusoidal cycle, to the peak acceleratory values. The computed gains, normalized to the resting rate, were 1.95–4.34% per deg·s^{-2} for the first peak and 1.71–3.69% for the mean peak response over several cycles. Similarly, the gains were 1.13–2.41% for the number of EPSPs in the first cycle and 1.09–2.12% over several cycles. Comparison of the gain for the first cycle to that for the whole rotation yielded a quantitative estimate of adaptation of EPSP response (4–32%).

The other four fibers exhibited a nonlinear intensity function during excitation. In these nonlinear fibers regression lines were computed by relating first-cycle and overall peak rates, as well as numbers of EPSPs, to the logarithm of acceleration.

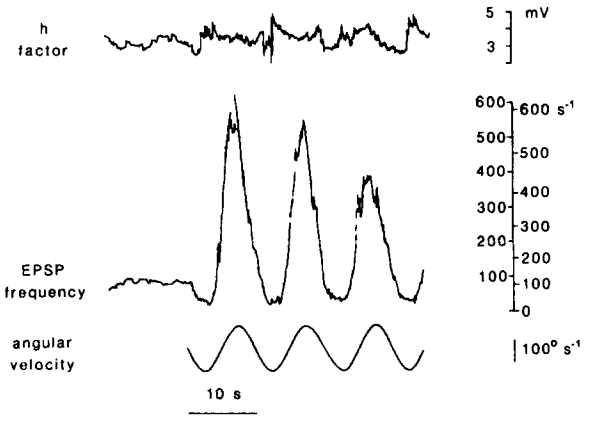

FIGURE 6. Example of measurements of EPSP amplitude (*upper trace*) and rate of occurrence (*middle trace*) using an averaging window of 2.5 instead of 5 s. Bottom trace is the turntable angular velocity. The measurement was performed on the same data as in Fig. 5 *D*. See legend of Fig. 5 for the vertical scales. Notice that differences between peak values obtained with the two windows are small. The shorter window reproduces more accurately the time course of the response in EPSP rate, but all estimates show wider fluctuations with time. This is particularly evident in the measurements of *h*, where the discontinuities due to giant events (already noticeable with the 5-s window for strong stimulations, as seen in Fig. 5, *C* and *D*) make the tracing markedly more noisy.

The slopes yielded the following estimated gains, expressed as changes (normalized to the resting levels) per *e*-fold increase in acceleration: 20.2–116.3% and 12.4–86.0% for the first and mean peak rates, respectively; 14.8–76.2% and 13.6–56.3% for the number of EPSPs during the first cycle and over the entire duration of stimulation. Also in these nonlinear units adaptation was demonstrated by the lower slopes observed for the overall values than for the initial ones (2–48% adaptation).

Measurements of EPSP Rate during Inhibitory Rotation

When the parameters used to quantify the excitatory response were used to describe the EPSP properties during inhibition, linear and nonlinear behaviors were also displayed by the different units.

In some units the decrease in EPSP rate with respect to the resting level was linearly related to the stimulus intensity. Regression lines of negative peaks in EPSP rate vs. peak acceleration yielded gains (expressed as percentage of the resting level per deg·s^{-2}) of 0.3–0.76% and 0.3–0.75% for the initial and mean inhibitory peaks, respectively. In the same units the total numbers of EPSPs during the inhibitory phase of the first sinusoidal cycle and over the entire duration of the stimulation period were also linearly related to acceleration, with gains of 0.22–0.45% and 0.20–0.41%, respectively.

In the nonlinear units the first and the mean inhibitory peaks were proportional to the logarithm of acceleration, with negative slopes of 11.7–26.3% and 9.7–37.0% of resting value per *e*-fold increase in inhibitory acceleration. Similarly, when the numbers of EPSPs were considered, negative slopes of 10.7–13.3% and 14.3–19.1% were obtained for the first inhibitory cycle and for the whole inhibitory response, respectively. No consistent adaptation of the response was observed during inhibition.

The Input-Output Intensity Function

In terms of the overall input-output intensity function, in one unit all the parameters examined were linearly related to acceleration; in another unit all the response parameters were related to the logarithm of acceleration; three fibers displayed linear behavior during excitation and nonlinear response during inhibition, and the situation was reversed in the remaining three units. Fig. 7 illustrates the response of the linear unit (*A*) and of the nonlinear one (*B*). The upper part of the figure illustrates the relation of excitatory and inhibitory peaks in EPSP rate to peak accelerations, whereas the number of EPSPs gained or lost during stimulations, with respect to the resting activity, are considered in the lower part of the figure. Two more examples of transduction characteristics, relating the first peak rates to the peak accelerations, are shown in Fig. 8. One of these units is linear during excitation and nonlinear during inhibition (*circles*); the opposite is true for the other unit (*triangles*).

In all units shown, however, the asymmetry between excitation and inhibition is evident, the excitatory response being systematically larger than its inhibitory counterpart when the canal is subjected to equivalent stimuli with opposite polarity. Thus, nonlinear characteristics are obtained for all fibers when both excitation and inhibition are considered.

Phase Behavior and Distortions in EPSP Response

The excitatory and inhibitory responses were generally in phase with angular velocity, although the EPSP peak response appeared to lead peak velocity by some 10–27 degrees. Thus at 0.1 Hz the synaptic output from the semicircular canal relays to the central vestibular neurons information more closely in phase with head velocity than head acceleration.

No consistent difference was observed between the times taken by the EPSPs to reach their maximum rate starting from the resting level and to recover the resting frequency from the peak, during rotation at 87 deg·s^{-2}, at difference with the skewness described in the generator potential (Taglietti et al., 1977).

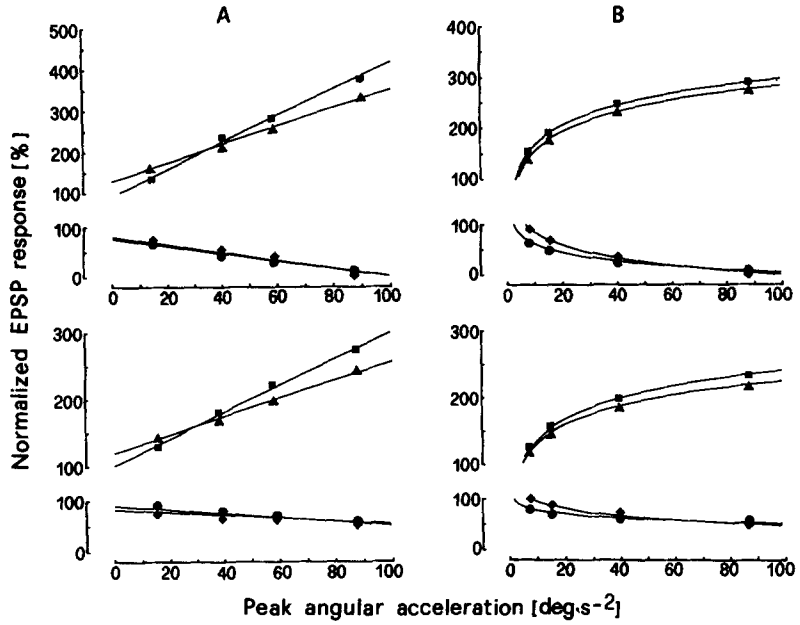

FIGURE 7. Responses of EPSP rate to sinusoidal rotation at 0.1 Hz in two different units (*A* and *B*), related to the peak values of acceleration. (*Top*) Excitatory (■ and ▲) and inhibitory (● and ♦) peaks in EPSP rate normalized to the resting levels. (*Bottom*) Total numbers of EPSPs occurring during the excitatory and inhibitory phases, normalized to the number of EPSPs during equal periods of spontaneous activity. Asymmetry of the responses is evident. In all panels, ■ and ● refer to responses during the first cycle of stimulation, whereas ▲ and ♦ refer to average responses over several cycles. Differences between the two groups of observations reflect adaptation, which is more evident for excitatory responses. Notice that the unit illustrated in *A* responds linearly with acceleration, whereas that in *B* responds linearly with the logarithm of acceleration. Continuous lines are least-squares fits.

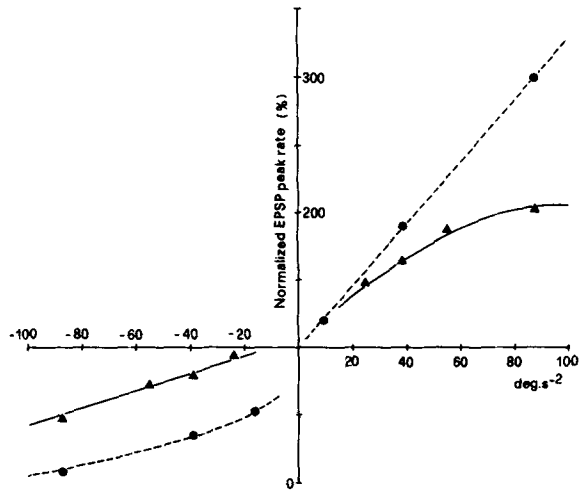

FIGURE 8. Two-sided input-output intensity functions for two different units. The peaks in EPSP rate during the first excitatory and inhibitory half-cycles, normalized to resting activity, are related to peak acceleration. One unit displays excitatory responses linear with acceleration and inhibitory responses linear with the logarithm of acceleration (●); the converse is true for the other unit (▲). Considered as a whole, the input-output intensity function is nonlinear for both units (fit drawn by eye).

Correlation of EPSP Rate with Spike Rate

The results reported above indicate that asymmetry and nonlinearity in the response, adaptation, and possibly the phase lead are intrinsic features of presynaptic mechanisms. However, the rectification described for the spike discharge was not observed at the level of EPSP response. To confirm these findings, it seemed appropriate to attempt a simultaneous, though limited, study of EPSP and spike activities in the same fiber. To this purpose recordings were obtained from fibers not exposed to TTX, at rest and during stimulation by rotation at 0.1 Hz with 40 deg·s^{-2} peak acceleration. 40-s recordings were acquired by the computer at a sampling rate of 1.6 kHz, and computations were performed offline on the digitized records. Spikes were recognized, counted and cancelled from the digital records; EPSP rate was then computed using the procedure described above, with a 2.5-s averaging window.

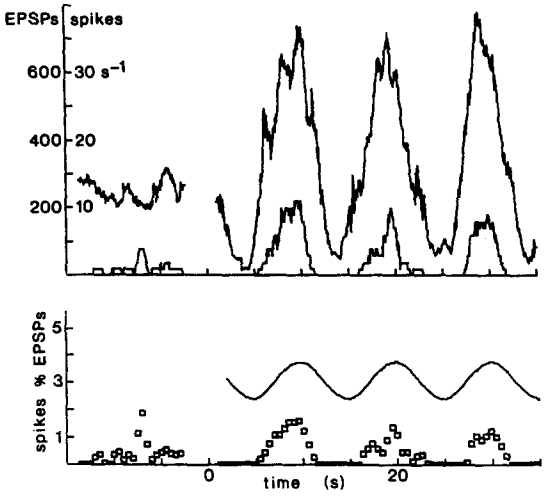

FIGURE 9. Simultaneous measurement of EPSP and spike rates from a single unit at rest and during stimulation by sinusoidal rotation at 0.1 Hz with 40 deg·s^{-2} peak acceleration. (*Top*) EPSP rate (the noisier trace) and spike rate (the trace closer to zero). The lower panel shows the number of spikes per 100 EPSPs together with the angular velocity of the turntable that marks the time scale and the period of stimulation. Notice that, as EPSP rate increases, spike rate as well as the number of spikes per 100 EPSPs rise. Notice also that spike firing begins to decline prematurely with respect to EPSP rate.

Five units were studied, and the results from one of them are shown as an example in Fig. 9. The main features of EPSP and spike responses illustrated in the figure were observed consistently in all five units, although the absolute values of EPSP and spike rates varied from one unit to the other. They may be summarized as follows: (*a*) resting spike rates were generally very low, only one fiber displaying a resting spike rate >3 s^{-1}; (*b*) during the excitatory phase of the stimulation, while EPSP rate was rising, spike rate increased even faster (i.e., the number of spikes per 100 EPSPs also increased); (*c*) the decline in spike rate generally anticipated that of EPSP rate, after the excitatory peak, so that the peak spike rate often preceded the peak EPSP rate by some 0.5–1 s. This apparent phase lead of spike firing was more consistently observed during the first cycle of stimulation; (*d*) fibers with low resting spike rates showed marked rectification of the response, spikes being abolished dur-

ing the whole inhibitory cycle, and a nonrectified response (though markedly asymmetrical) was exhibited by only one unit, which had a resting spike frequency of $\sim 4\ s^{-1}$.

DISCUSSION

To our knowledge, this study is the first attempt to describe the static and dynamic properties of transmitter secretion at the afferent synapse in the semicircular canals. The resulting information helps to dissect the characteristics of the afferent spike discharge due to presynaptic processes at the cyto-neural junction from those arising at the encoder. Both structures contribute to the afferent spike pattern, whose parameters have been exclusively employed up to now to define the canal transfer function.

Although direct generalizations to the whole population of afferent fibers may not be granted by the size of the sample analyzed here, convincing evidence has been provided that the afferent synapse does not merely reproduce the torsion pendulum model, which predicts a mere low-pass filter behavior.

Statistical Analysis of EPSP Noise

The procedure of fluctuation analysis used in this study was tailored to continuously monitor the rapidly changing parameters of EPSP activity. The good agreement of estimates of EPSP amplitude with the values obtained from amplitude histograms of single events, and the general consistency and smoothness of continuous measurements of the h parameter within single units, indicate that the procedure is reliable and is not invalidated by relatively rapid changes in the parameters of the process under study. Direct counts of EPSPs in the presence of rates up to $100\ s^{-1}$ confirm the accuracy of the procedure. It appears therefore that the statistical approach can be employed even in the face of biological processes that depart under many respects from the ideal, uniform, linear, and stationary shot noise for which fluctuation analysis was devised in the beginning. The procedure so constitutes a valuable and versatile tool for the study of synaptic and cellular physiology.

The analysis of the power spectra of EPSP noise and the successful reconstitution of the waveform of the single event (shot) from the spectra, based on the minimum-phase assumption, indicate that the postsynaptic noise is constituted by the summation of randomly occurring shots with the same general waveform as the isolated EPSPs. Furthermore, the shots can be considered as uncorrelated, homogeneous and occurring at a stationary rate, at least as far as it is needed for our measurements. We refer to these shots as EPSPs. Indeed, the shots might as well be truly unitary synaptic events, i.e., miniature EPSPs related to the release of single quanta of neurotransmitter. The unimodal distributions observed for EPSP amplitudes suggest that this is the case. On the contrary, the relevant mean value, broadness, and skewness of the amplitude distribution of the shots tend to suggest that they are multiquantal events, i.e., EPSPs strictly speaking. In both cases, unimodal, broad, and smooth amplitude distributions might arise from the fact that the EPSPs generated at multiple synapses on the nerve terminals of a single axon may undergo variable amounts of electrotonic decrement as well as different degrees of temporal summation, before reaching the recording site, located ~500 μm away from the

junction, in a position where, most likely, the peripheral axon twigs have already converged into the fiber main stem.

The marked differences in EPSP rates among different units may be related to the possible convergence of a variable number of hair cells on a single afferent axon, as it was suggested for the spike discharge frequency (Taglietti et al., 1973; Hartmann and Klinke, 1980; Rossi and Martini, 1986*a*). The high frequency of the subthreshold events may also be sustained by multiple release sites from a single hair cell, as it was suggested in the goldfish sacculus (Furukawa and Matsuura, 1978).

The Asymmetry of EPSP Response

Our central finding is that, although the resting EPSP rate is sufficiently high to provide a convenient level of bidirectional modulation by the mechanical stimulus, asymmetry between excitation and inhibition is invariably observed for accelerations larger than 40 deg·s^{-2}. The excitatory response is more conspicuous than its inhibitory counterpart, not only when peak values are considered but also when the total increase in the number of EPSPs during the excitatory phase of stimulation is compared with the decrease during the corresponding inhibitory phase. The hair cell response is roughly linear for displacements of the hair bundle tip up to 400 nm (Hudspeth and Corey, 1977). The hydrodynamic properties, calculated according to Bernard (1982) for our system (Rossi and Martini, 1986*b*), indicate that the stimuli applied in this study produced hair-tip deflections <52 nm. Therefore, even allowing for a wide margin of error in the latter estimate, the asymmetry observed here (up to fivefold ratio between excitatory and inhibitory responses) is most probably related to further steps in the modulation of synaptic activity.

At difference with the described spike behavior, the most sensitive units during excitation showed larger inhibitory responses as well, independently of the resting EPSP rates. Rectification in EPSP response was never observed, in accord with the finding that no rectification occurs in the generator potential measured at the frog posterior canal, during rotation at 0.1 Hz with peak accelerations as high as 119 deg·s^{-2} (Taglietti et al., 1977). This indicates that rectification is a property of the spike generation mechanism.

The Input-Output Intensity Function

Because of asymmetry in the response, intensity functions over both excitation and inhibition were nonlinear for all fibers. For some of the fibers studied, the input-output intensity function was not linear even considering either excitation or inhibition alone.[3] In these cases the parameters of the response appeared to be linearly related to the logarithm of peak acceleration. This may determine the linear and logarithmic spike responses previously described for different fibers (Fernandez and Goldberg, 1971; Precht et al., 1971; Blanks and Precht, 1976; O'Leary and Honrubia, 1976; Correia et al., 1977; Segal and Outerbridge, 1982 *a* and *b*; Rossi and

[3] It may be appropriate to observe here that the classification in linear and nonlinear fibers held before as well as after correcting estimated EPSP rates for nonlinear summation of the events, i.e., the latter phenomenon did not interfere with the definition of the input-output function. This makes us more confident on the validity of the fluctuation analysis procedure and the reliability of the intensity functions obtained.

Martini, 1986*a*). As stated above, by assuming that, under the conditions of weak stimulation here examined, the receptor potential behaves as an essentially linear element in the afferent response cascade system, at least part of the nonlinearity must arise at some subsequent presynaptic step. This possibility has never been considered explicitly in previous studies on peripheral vestibular physiology: mechanoelectrical transduction and the encoder are the possible sources for the nonlinear intensity function considered so far with most attention (see Segal and Outerbridge, 1982).

Adaptation in EPSP Response

Spike-discharge adaptation is commonly described in a consistent fraction of the afferent fiber population (Fernandez and Goldberg, 1971; Precht et al., 1971; Blanks and Precht, 1976; O'Leary and Honrubia, 1976; Correia et al., 1977; Segal and Outerbridge, 1982 *a*, *b*; Kuno, 1983; Rossi and Martini, 1986*a*). Although adaptation of the receptor response has been reported (Eatock et al., 1987), it is rapid (with a time constant in the order of tens of milliseconds) with respect to our time scale. Long-term adaptation of receptor response, though never described, may also be present. Further possible sources of adaptation include intervening changes in basolateral conductances and fatigue of synaptic transmission, as was suggested for EPSPs in the goldfish sacculus (Furukawa and Matsuura, 1978; Furukawa et al., 1978).

In this study, we observed adaptation in the EPSP rate, which became evident during prolonged rotation and increased with increasing accelerations. In the absence of adaptation of the inhibitory response, this resulted in a decrease in overall synaptic activity with time, which paralleled the intensity of stimulation. This is consistent with the idea that EPSP response adaptation reflects fatigue of the afferent synapse, possibly due to depletion of quanta from the immediately available transmitter store. Reduced transmitter output can account for the observed decline in spike rate. Further contribution may arise from electrogenic sodium pumping, which is activated after intense stimulation of the semicircular canal (Taglietti et al., 1977).

The Relation of EPSP Rate to Spike Firing

The resting EPSP frequency is considerably higher than the spontaneous spike rates (maximal rates 30 s^{-1} with 90% of the units firing between 0 and 7 spikes$\cdot s^{-1}$; Rossi and Martini, 1986*a*). Because spike rate is presumably related to the probability that the fluctuating signal generated by the summation of EPSPs reaches the threshold for firing, the relation between spike and EPSP rates is expected not to be linear, and rectification (silencing of spike firing) to occur for low EPSP rates. In the few units where we studied EPSP and spike rates concomitantly, we confirmed the nonlinearity of the relation, leading to amplification of the asymmetry in the response, and the rectification by the encoder. However, the relation of spike rate to EPSP frequency is not static. In particular, the premature fall in spike rate indicates that the postsynaptic mechanisms implied in spike generation have complex dynamic properties. Excitatory and inhibitory peaks in EPSP rate show a variable phase lead with respect to the peak turntable angular velocity (10–27 degrees), which is in

agreement with the observed phase lead of spike rate (Blanks and Precht, 1976). The premature fall of spike rate during excitation may introduce an apparent further phase lead. Possible causes of this phenomenon include anticipated repolarization during excitation due to the activation of the sodium pump (Taglietti et al., 1977), and partial inactivation of sodium channels.

A much deeper study of the relation between spike and EPSP rates, under different conditions of stimulation, will be necessary to describe in detail the mechanism and the dynamic behavior of the encoder. This, however, would go beyond the purposes of the present work.

APPENDIX

Analysis of Simulated Recordings

The analytical function describing EPSP waveform, $w(t)$, was computed at 60-μs intervals using values for τ and γ chosen within the range of experimentally observed values. A deterministic function was then defined (a constant plus either a sinusoidal wave or an asymmetrical sinusoid) to describe the time course of the expected rate of occurrence of the events, $r(t)$. The asymmetrical sinusoid was obtained by adding a sinusoid to a fraction of its own absolute value, thus obtaining larger peaks in the positive than in the negative direction. In the various runs of simulation, $r(t)$ ranged from 60 to 1,250 s^{-1}. From the instantaneous value of $r(t)$, a Poisson number generator program determined the number of events occurring in each elementary interval (0.3 ms), and a digital record was created by summating the waveforms of all occurring events. The amplitude parameter (h) was chosen arbitrarily in each run with the aim of exploiting the full range of the digital to analog converter (4,096 bins) without overflowing. The digital record thus obtained was output in real time by the computer as an analog signal, and was recorded on tape and further analyzed like the experimental recordings.

The estimated values of h fell between 0.8 and 1.3 times the input value, spending at least 80% of the time between 0.9 and 1.1. In general, the values did not fluctuate much within a single recording, indicating that the averaging period (5s) was sufficiently long to keep random errors within reasonably narrow limits. The estimated values of EPSP rates, expressed as fractions of the corresponding input values ± SD, were: 0.98 ± 0.08 for maxima in EPSP rate, 1.13 ± 0.18 for minima, and 0.94 ± 0.09 for the peak to peak difference within each cycle. The times of the positive and negative peaks of EPSP rate, as measured on chart records of the output were in error by <0.2 s (±0.4 s, SD).

The measured time courses of EPSP rates indicate that a cycle constituted by a 5-s strong excitatory response plus a 5-s weak inhibitory response becomes smoothed by a 5-s window to a more or less symmetrical sinusoid, with an apparent shift toward a higher resting level. This is due to removal of even harmonics by a window with duration equal to half the fundamental period. Although valid estimates are obtained for maximum, minimum, and peak-to-peak rates, and for the areas under the positive and negative half-periods, the system appears to paradoxically spend more than half of the cycle in the excitatory state, i.e., at rates higher than the resting value, as observed in the chart recordings obtained from experimental data (Fig. 5).

When the simulations of asymmetrical time courses of EPSP rate were reanalyzed using an averaging window duration of 2.5 s (one-fourth of a cycle), a more noisy record was obtained for EPSP rate, but its true time course was reproduced more accurately. The duration of excitation and inhibition (i.e., the time spent by EPSP rate over and below its simulated resting value) became roughly equal and the sinusoidal changes in estimated EPSP rate became clearly asymmetrical, with the positive lobe noticeably higher than its negative counterpart.

We dedicate this paper to Prof. Cesare Casella, Head of the Institute of General Physiology of the University of Pavia, on the occasion of his 70th birthday.

This work was supported by grants from Consiglio Nazionale delle Ricerche and from Ministero della Pubblica Istruzione, Roma, Italy.

Original version received 11 July 1988 and accepted version received 21 February 1989.

REFERENCES

Bendat, J. S., and A. G. Piersol. 1971. Random Data: Analysis and Measurement Procedures. John Wiley & Sons, New York. 407 pp.

Bernard, C. 1982. Theoretical aspects of cupula deflection in semicircular canal. *Journal of Theoretical Biology.* 98:637–643.

Blanks, R. H. I., and W. Precht. 1976. Functional characterization of primary vestibular afferents in the frog. *Experimental Brain Research.* 25:369–390.

Ceccarelli, B., R. Fesce, F. Grohovaz, and C. Haimann. 1988. The effect of potassium on exocytosis of transmitter at the frog neuromuscular junction. *Journal of Physiology.* 401:163–183.

Correia, M. J., J. P. Landolt, M. D. Mi, A. R. Eden, and J. L. Rae. 1977. A species comparison of linear and nonlinear transfer characteristics of primary afferents innervating the semicircular canal. *In* The Vestibular System: Function and Morphology. T. Gualtierotti, editor. Springer Verlag, New York. pp. 280–316.

Eatock, R. A., D. P. Corey, and A. J. Hudspeth. 1987. Adaptation of mechanoelectrical transduction in hair cells of the bullfrog's sacculus. *Journal of Neuroscience.* 7:2821–2836.

Fernandez, C., and J. M. Goldberg. 1971. Physiology of peripheral neurons innervating semicircular canals of the squirrel monkey. II. Response to sinusoidal stimulation and dynamics of peripheral vestibular system. *Journal of Neurophysiology.* 34:661–675.

Fesce, R., J. R. Segal, B. Ceccarelli, and W. P. Hurlbut. 1986*a*. Effects of black widow spider venom and calcium on quantal secretion at the frog neuromuscular junction. *Journal of General Physiology.* 88:59–81.

Fesce, R., J. R. Segal, and W. P. Hurlbut. 1986*b*. Fluctuation analysis of nonideal shot noise. Application to the neuromuscular junction. *Journal of General Physiology.* 88:25–57.

Fuortes, M. G. F., and A. L. Hodgkin. 1964. Changes in time scale and sensitivity in the ommatidia of *Limulus*. *Journal of Physiology.* 172:239–263.

Furukawa, T., Y. Hayashida, and S. Matsuura. 1978. Quantal analysis of the size of excitatory postsynaptic potentials at synapses between hair cells and afferent nerve fibres in goldfish. *Journal of Physiology.* 276:211–226.

Furukawa, T., and S. Matsuura. 1978. Adaptive rundown of excitatory post-synaptic potentials at synapses between hair cells and eighth nerve fibres in the goldfish. *Journal of Physiology.* 276:193–209.

Haimann, C., F. Torri-Tarelli, R. Fesce, and B. Ceccarelli. 1985. Measurement of quantal secretion induced by ouabain and its correlation with depletion of synaptic vesicles. *Journal of Cell Biology.* 101:1953–1965.

Hartmann, R., and R. Klinke. 1980. Discharge properties of afferent fibres of the goldfish semicircular canal with high frequency stimulation. *Pflügers Archiv.* 338:111–121.

Heiden, C. 1969. Power spectrum of stochastic pulse sequences with correlation between the pulse parameters. *Physical Review.* 188:319–326.

Hudspeth, A. J., and D. P. Corey. 1977. Sensitivity, polarity and conductance change in the response of vertebrate hair cells to controlled mechanical stimuli. *Proceedings of the National Academy of Sciences.* 74:2407–2411.

Hudspeth, A. J., and R. S. Lewis. 1988*a*. Kinetic analysis of voltage and ion-dependent conductances in saccular hair cells of the bull-frog, *Rana catesbeiana. Journal of Physiology.* 400:237–274.

Hudspeth, A. J., and R. S. Lewis. 1988*b*. A model for electrical resonance and frequency tuning in saccular hair cells of the bull-frog, *Rana catesbeiana. Journal of Physiology.* 400:275–297.

Kuno, M. 1983. Adaptive changes in firing rates in goldfish auditory fibers as related to changes in mean amplitude of excitatory postsynaptic potentials. *Journal of Neurophysiology.* 50:573–581.

Martin, A. R. 1955. A further study of the statistical composition of the endplate potential. *Journal of Physiology.* 130:114–122.

O'Leary, D. P., and V. Honrubia. 1976. Analysis of afferent responses from isolated semicircular canal of the guitarfish using rotational acceleration white-noise inputs. II. Estimation of linear system parameters and gain and phase spectra. *Journal of Neurophysiology.* 39:645–659.

Papoulis, A. 1962. The Fourier integral and its applications. McGraw-Hill Book Co., New York. 318 pp.

Peterson, C. W., and B. W. Knight. 1973. Causality calculations in the time domain: an efficient alternative to the Kramers-Kronig method. *Journal of the Optical Society of America.* 63:1238–1242.

Precht, W. R., R. Llinás, and M. Clarke. 1971. Physiological responses of frog vestibular fibers to horizontal angular rotation. *Experimental Brain Research.* 13:378–407.

Rice, S. O. 1944. Mathematical analysis of random noise. *Bell Telephone System Journal.* 23:282–332.

Rossi, M. L., and M. Martini. 1986*a*. Afferent activity recorded during rotation from single fibres of the posterior nerve in the isolated frog labyrinth. *Experimental Brain Research.* 62:312–320.

Rossi, M. L., and M. Martini. 1986*b*. Some hydrodynamic properties of the posterior canal in the frog labyrinth related to neuronal responses. *Neuroscience Letters.* 66:328–332.

Rossi, M. L., and M. Martini. 1988. The effect of barium and some channel blockers on sensory discharge of the frog labyrinth posterior canal recorded at rest and during rotation. *Brain Research.* 452:312–322.

Rossi, M. L., I. Prigioni, P. Valli, and C. Casella. 1980. Activation of the efferent system in the isolated frog labyrinth: effects on the afferent EPSPs and spike discharge recorded from single fibres of the posterior nerve. *Brain Research.* 185:125–137.

Rossi, M. L., P. Valli, and C. Casella. 1977. Post-synaptic potentials recorded from afferent nerve fibres of the posterior semicircular canal in the frog. *Brain Research.* 135:67–75.

Schick, K. L. 1974. Power spectra of pulse sequences and implications for membrane fluctuations. *Acta Biotheoretica.* 23:1–17.

Segal, B. N., and J. S. Outerbridge. 1982*a*. Vestibular (semicircular canal) primary neurons in bullfrog: nonlinearity of individual and population response to rotation. *Journal of Neurophysiology.* 47:545–562.

Segal, B. N., and J. S. Outerbridge. 1982*b*. A nonlinear model of semicircular canal primary afferents in bullfrog. *Journal of Neurophysiology.* 47:563–578.

Segal, J. R., B. Ceccarelli, R. Fesce, and W. P. Hurlbut. 1985. Miniature endplate potential frequency and amplitude determined by an extension of Campbell's Theorem. *Biophysical Journal.* 47:183–202.

Steinhausen, W. 1931. Über den Nachweis der Bewegung der Cupula in der intakten Bogengaengsampulle des Labyrinths bei der natürlichen rotatorischen und calorischen Reizung. *Pflügers Archiv.* 228:322–328.

Steinhausen, W. 1933. Über die Beobachtung der Cupula in den Bogengaengsampullen des Labyrinths des lebenden Hechts. *Pflügers Archiv.* 232:500–512.

Taglietti, V., M. L. Rossi, and C. Casella. 1977. Adaptive distortions in the generator potential of semicircular canal sensory afferents. *Brain Research.* 123:41–57.

Taglietti, V., P. Valli, and C. Casella. 1973. Discharge properties and innervation of the sensory unit in the crista ampullaris. *Archivio di Scienze Biologiche.* 57:73–86.

Valli, P., and G. Zucca. 1976. The origin of slow potentials in semicircular canals of the frog. *Acta Otolaryngologica.* 81:395–405.

Wong, F., and B. W. Knight. 1980. Adapting-bump model for eccentric cells of *Limulus*. *Journal of General Physiology.* 76:539–557.